DOI: 10.13009/EUCASS2023-398
Aerospace Europe Conference 2023 – 10TH EUCASS – 9TH CEAS

DNS of flow in pipes with large relative roughness height

Mariangela De Maio[⋆†], *Beatrice Latini*[⋆], *Francesco Nasuti*[⋆] *and Sergio Pirozzoli*[⋆]
[⋆]*Dipartimento di Ingegneria Meccanica e Aerospaziale, Sapienza Universitá di Roma*
via Eudossiana 18, 00184 Roma, Italia
mariangela.demaio@uniroma1.it · beatrice.latini@uniroma1.it ·
francesco.nasuti@uniroma1.it · sergio.pirozzoli@uniroma1.it
[†]Corresponding author

Abstract

We carry out direct numerical simulations (DNS) of turbulent flow in rough pipes, to investigate the influence of large relative roughness on both momentum and heat transfer. Two types of irregular roughness are studied, namely a grit-blasted and a graphite surface. Simulations are conducted across various Reynolds numbers, spanning from laminar to fully rough conditions, while maintaining a constant molecular Prandtl number of 0.7. Despite the large relative roughness, the results closely follow those of Nikuradse and a logarithmic region in the streamwise velocity profiles can still be highlighted. Nevertheless, the flow retains an influence on the rough duct cross-sectional shape. Indeed, the values of the friction coefficient in the laminar region differs of about $7-9\%$ from the theoretical values. Furthermore, we found differences between the velocity roughness function computed for the pipe and the one obtained for a flat channel with identical wall roughness. Variations can be observed between the velocity and temperature fields, resulting in velocity roughness functions that are larger in comparison to the temperature roughness functions. The aforementioned differences arise due to the decrease in heat exchange efficiency as Reynolds number increases, causing the breakdown of the Reynolds analogy.

1. Introduction

Pressure-driven flow in ducts is a subject of utmost relevance in mechanical and aerospace engineering applications. For instance, effective design of ducts in cooling systems of liquid rocket engines is extremely important because of the harsh environment to which the system is subjected, which also mandates the use of advanced numerical simulations as design tool. The present authors[27] have recently carried out a numerical study of flow in smooth rectangular cooling ducts, and found that, whereas traditional approaches as RANS (Reynolds-averaged Navier-Stokes) yield good prediction of the pressure drop, the error in the prediction of the heat transfer coefficient may be as high as 20%. Furthermore, recent technological advances in the field of additive manufacturing have further prompted investigations of flow over surfaces with large relative roughness[6,40,41] . Additive manufacturing indeed allows to build three-dimensional objects starting from a digitized three-dimensional model and adding material such as plastics, liquids or powder grains being fused, typically layer-by-layer. This procedure allows for instance to machine cooling channels with more complex geometry and smaller size, however it also yields large relative roughness, which significantly affects both frictional drag and heat transfer.

So far, roughness has been investigated mainly by means of experimental studies. The systematic experimental investigation carried out by Nikuradse[29] is widely regarded as the starting point for the study of turbulent flows over rough walls. Nikuradse compiled an extensive database for fully developed flow in circular pipes whose walls were covered with unstructured roughness consisting of sieved sand grains. Nikuradse found that the presence of roughness affects both the mean flow and the turbulent motion of a fluid, which entails an increase of friction with respect to the smooth wall case. This is linked to the downward shift in the inner-scaled profile of the mean streamwise velocity, which can be expressed through the so called roughness function[14] ,

$$\Delta U^+ = U_S^+ - U_R^+ = \frac{1}{\kappa}\log k^+ + A - B(k^+), \tag{1}$$

where $\kappa(\approx 0.39)$ is the von Kármán constant, $A(\approx 5.0)$ is the log-law intercept for flow over smooth walls, and B is a function of both the roughness topography and the roughness Reynolds number k^+. The latter is defined as $k^+ = k/\delta_\nu$, where k is the roughness height and δ_ν is the friction length. We recall that $\delta_\nu = \nu/u_\tau$ and $u_\tau = \tau_w/\rho$, where ν is the viscosity of the fluid, τ_w is the shear stress at the wall and ρ is the density of the fluid.

DOI: 10.13009/EUCASS2023-398

In his experiments, Nikuradse found that the value of the roughness Reynolds number identified three flow regimes: hydraulically smooth, transitionally rough and fully rough. In the first regime the height of the roughness is of the order of the viscous sublayer, hence roughness does not affect the flow behavior, so k^+ is very small and $\Delta U^+ \approx 0$. In the transitionally rough regime, the behaviour of the flow and the trend of ΔU^+ plotted against k^+ depend strongly on the geometrical shape of the roughness. Finally, in the fully rough regime the friction coefficient is nearly unaffected by Reynolds number variations, while still depending on the roughness elements' shape and height. The fully rough regime is achieved for $\Delta U^+ > 7$, in which case the trend becomes independent of k^+, and the roughness function tends to align to the fully-rough asymptote. Most studies published to date aim at evaluating an equivalent sand-grain roughness k_s, which was first defined by Schlichting,[39] as the size of sand grains in Nikuradse's experiments which yields the same drag as the surface under consideration.
As for the velocity field, we can also define a temperature roughness function[20,21]

$$\Delta\Theta^+ = \Theta_S^+ - \Theta_R^+, \tag{2}$$

which is a function of both the roughness Reynolds number and the molecular Prandtl of the fluid. Unlike for the velocity roughness function, an asymptotic form of $\Delta\Theta^+$ has not been observed yet, even in the fully rough regime. Therefore, the equivalent sand-grain roughness is enough to predict momentum transfer, however we can not rely only on it for the prediction of heat transfer. This is due to the fact that roughness enhances heat transfer less than momentum transfer, meaning that efficiency in heat transfer decreases with respect to the smooth case. The latter result has been observed mainly experimentally. For instance, Dipprey and Sabersky[9] performed some tests inside pipes with granular close-packed roughness and found dependence of the heat transfer coefficient on the type of the roughness. Furthermore, they noticed that increases in the heat transfer coefficient are accompanied by even larger increases in the skin friction coefficient. Later, Bons[2] investigated real turbine blades, which were roughned by various degradation mechanisms, and they attributed the decrease of heat transfer efficiency to the obstacles of the rough surface, leading to a substantial generation of pressure drag. Nonetheless, there is no analogous mechanism, such as pressure, that influences heat transfer.
The last advancements in high performance computing have also brought attention to numerical simulations. The majority of these studies have been so far mainly focused on structured geometrical roughness, such as transversal and longitudinal bars[24] and sinusoidal elements[7] . In this regard, Leonardi et al.[24] investigated heat transfer inside a flow over geometrical bars and found that the temperature field near the wall is strongly dependent on the cross-sectional shape of the bars.
Realistic roughness has been lately investigated inside channels with an infinite extension in the streamwise direction. This is the case of Forooghi et al.[13] , who focused on the flow over rough surfaces of realistic combustion chamber deposits. They noticed that heat transfer is less enhanced with respect to friction as the Reynolds number increases. The same result was also found by Peeters et al.[34] , who performed DNS over grit-blasted surfaces with roughness of various heights and found that the Reynolds analogy hypothesis does not hold at high Reynolds numeber and large roughness height. According to that hypothesis, there is a similarity between the momentum and heat transfer characteristics of the flow. However, they found significant differences between the temperature and velocity statistics, indicating a decrease in heat transfer efficiency compared to the smooth wall case.
The numerical studies cited so far have focused on flows within channels of infinite transverse extension. Nevertheless, the presence of large roughness can affect the shape of the duct, leading to a dependence of the results on the cross-sectional geometry. Hence, the current study will employ DNS for the first time to replicate the flow dynamics within circular pipes with realistic roughness at the walls. The comparison of the present results with the ones obtained by Busse et al.[5] will allow for investigation of the dependence of the cross-sectional shape of the rough ducts. Indeed, Busse et al.[5] performed DNS inside plane channels with the same roughness as the one considered in the present research. Furthermore, the results will be compared with those obtained by Nikuradse, whose pipes have a maximum roughness height which is three times smaller than the one herein presented. However, the main goal of the present work will be to focus on the differences between momentum and heat transfer, aiming to understand how high roughness affects heat transfer efficiency. The simulations will be carried out with two different rough surfaces, a graphite and a grit-blasted samples. Last, a relatively wide range of Reynolds numbers is investigated and the Prandtl number is imposed equal to 0.7.

2. Metodology

2.1 Numerical method and definitions

A second-order finite-difference discretization of the incompressible Navier-Stokes equations in Cartesian coordinates is used, based on the classical marker-and-cell method[15,31] , with staggered arrangement of the flow variables to remove

DOI: 10.13009/EUCASS2023-398

odd-even decoupling phenomena and guarantee discrete conservation of the total kinetic energy in the inviscid flow limit. The Poisson equation resulting from enforcement of the divergence-free condition is efficiently solved by double trigonometric expansion in the streamwise and spanwise directions, and inversion of tridiagonal matrices in the third direction[22] . A hybrid third-order Runge-Kutta algorithm is used for time integration, whereby the convective terms are treated explicitly, and the diffusive terms are handled implicitly to alleviate the time step limitation. The flow is forced through a time-varying pressure gradient Π, such that the mass-flow-rate is strictly constant in time.
In the present study the Navier-Stokes equations are augmented with the transport equation for a passive scalar field, which from now on will be referred to as representative of the temperature field θ. Similarly to the streamwise velocity field, the passive scalar equation is also forced with a time-varying, spatially homogeneous forcing term Q, in such a way that the integral of the temperature over the pipe is strictly constant in time[35] .
In the present simulations the constant passive scalar value at the wall $\theta_w = 0$ is assigned as boundary condition in all the simulations. The computational domain is a rectangular box of size $L_x \times L_y \times L_z$, covered with a uniform Cartesian mesh. A rough pipe with mean radius R and cross-sectional area $A = \pi R^2$ is embedded in it, and the boundary conditions at the wall are approximately enforced through the immersed-boundary method. According to this method, as a preliminary step, the pipe geometry is generated in the standard Stereo-LiThography format, and a geometrical preprocessor based on the ray-tracing algorithm[33] is applied to discriminate grid points belonging to the fluid and the solid phase[17] . Near the fluid-solid interface the viscous terms dominate the nonlinear and pressure terms, hence the boundary conditions can be enforced by locally changing the finite-difference weights for the approximation of the second derivatives[32] . The predictive capability of the method for the numerical simulation of turbulent flows over rough surfaces was documented in a large number of papers[1,3,17,32] .
The controlling parameter of the flow is the bulk Reynolds number $Re_b = 2Ru_b/\nu$, where

$$u_b = \frac{1}{V}\int_V U\, dV, \tag{3}$$

is the bulk velocity, with U the mean streamwise velocity and V is the fluid volume. The resulting friction Reynolds number is $Re_\tau = Ru_\tau/\nu$, where the friction velocity is evaluated based on the measured pressure gradient, $\tau_w = R/2\,\langle\Pi\rangle$.
The bulk temperature is defined as

$$\Theta_b = \frac{1}{u_b V}\int_V U\theta\, dV. \tag{4}$$

For normalization of the temperature field we will consider the friction temperature,

$$\Theta_\tau = \frac{\langle q_w\rangle}{u_\tau} = \frac{R}{2}\frac{\langle Q\rangle}{u_\tau}, \tag{5}$$

where $\langle q_w\rangle$ is the heat flux at the wall. The resistance that the fluid encounters inside the pipe is quantified through the friction factor, defined as

$$C_f = 2\tau_w/(\rho u_b^2), \tag{6}$$

where τ_w is the wall shear stress and ρ is the density. Whereas the overall heat transfer performance of the duct is quantified in terms of the Stanton number,

$$St = \frac{\langle q_w\rangle}{\rho C_p u_b(\theta_w - \Theta_b)}, \tag{7}$$

In this case, the non-dimensional form for (7) is adopted, thus the density ρ and the specific heat C_p are equal 1.
Hereafter, capital letters are used to denote flow properties averaged in the streamwise direction and in time. The + superscript is here used to denote wall units, namely quantities made nondimensional with respect to the friction velocity, temperature and the viscous length scale.

2.2 Geometries

Two types of rough surfaces are considered, both downloades from the University of Southampton Institutional Repository[42] . The first one, shown in figure 1 (a), derives from the scan of a grit-blasted surface, and the second one, shown in figure 1 (b), derives from a sample of graphite. In both cases, the surfaces have been scanned and then a post-procedure has been applied to remove the tilting and the curvature of the surface. Last, a low-pass Fourier filter was applied to the scanned roughness profiles. The filtering serves a dual purpose, to remove the noise due to the scanning process and, secondly, to make the surface periodic, thereby enabling the imposition of numerical boundary conditions

DOI: 10.13009/EUCASS2023-398

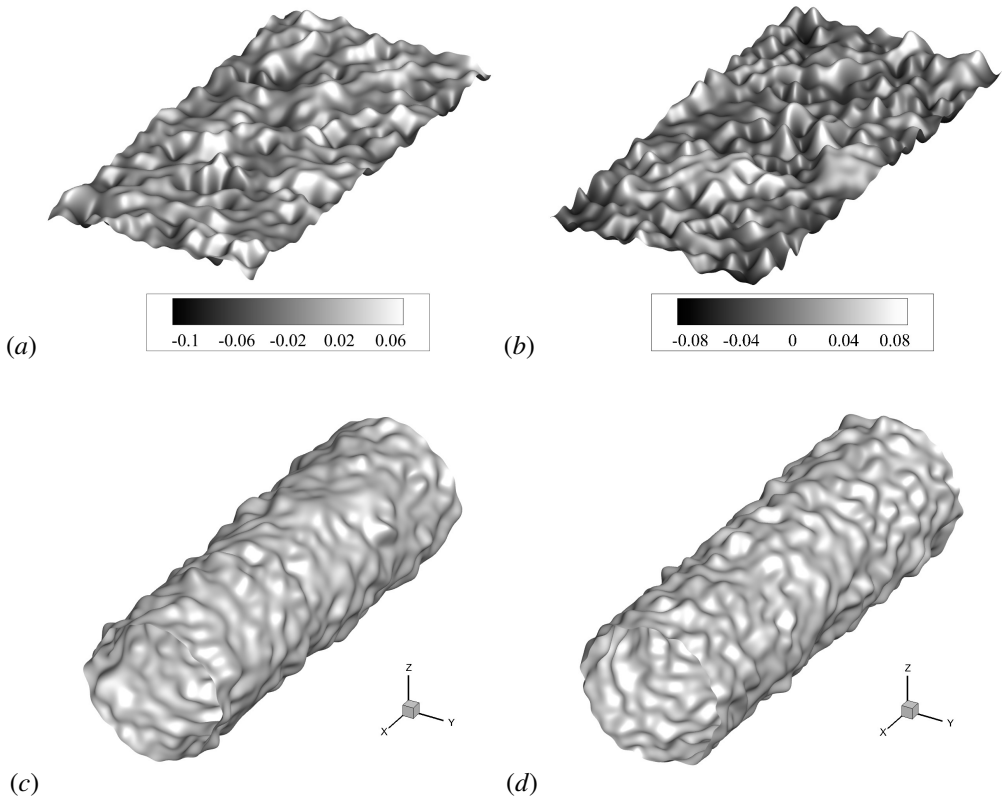

Figure 1: Topography of rough surfaces. Panels (*a*) and (*b*) show the geometries of grit-blasted surface and graphite surface, originally used for channel flow of Busse et al.[5] and Peeters et al.[34] , with color map showing the elevation normalized by the channel half-height. Panels (*c*) and (*d*) show the geometries obtained by wrapping the original rough surfaces around the pipe as explained in the text.

in the streamwise direction. Full information about the database is available in Thakkar et al.[43] . The rough pipe geometries shown in panels (*c*) and (*d*) were then obtained by doubling the baseline samples in the spanwise direction, and wrapping the surfaces thus obtained around the mean pipe geometry. In the present study we define the roughness height to be the mean-peak-to-trough height (k), as obtained by partitioning the surface into 5×5 tiles of equal size, and then computing the average of the difference between the maximum and minimum height for each tile.[43] The relative roughness height is $k/R = 0.186$ for the grit-blasted surface and $k/R = 0.199$ for the graphite surface. It is also important to note that in the forthcoming presentation of the results, the wall distance y is measured from the mean plane of the rough surface, hence negative y are allowed.

2.3 Set-up

In this section, the input parameters and corresponding results are presented, as outlined in table 1.
The pipe length is about $L_x = 6.27R$, in both cases. The computational domain in the cross-stream directions measures $L_y = L_z = 2.45R$, for the grit-blasted surface, and $L_y = L_z = 2.29R$, for the graphite surface.
Through a series of preliminary studies, the impact of the pipe length on the computed results has been examined. DNS in axially doubled domains have in fact shown that the baseline domain is enough to obtain accurate results.
Furthermore, we have carried out a grid sensitivity analysis at $Re_b = 4400$, for both roughness geometries, which has shown that at least $N_x = 384$ grid points should be used along the streamwise direction, and $N_y = N_z = 192$ grid points should be used in the transversal directions. This would correspond to about fifteen grid points per roughness element, thus corroborating the findings of Busse et al.[4] . The number of grid points has been progressively increased with the Reynolds number, and we have verified that the grid resolution is adequate also at $Re_b = 30000$.
The time step expressed in wall units (ν/u_τ^2) ranges from about $\Delta t^+ = 0.015$ for the cases at $Re_b = 500$ to about $\Delta t^+ = 0.29$ for the cases at $Re_b = 30000$. The time intervals used to collect the flow statistics are also reported in table 1 in terms of eddy-turnover times ($\tau_t = R/u_\tau$). They are typically much longer than the current practice in DNS

DOI: 10.13009/EUCASS2023-398

Grit-blasted										
Re_b	Re_τ	k^+	$C_f \times 10^2$	$St \times 10^3$	N_x	$N_y = N_z$	Δx^+	$\Delta z^+ = \Delta y^+$	T/τ_t	Symbol
500	32.75	6.08	3.43	17.09	384	192	0.53	0.42	104.77	
1000	46.69	8.70	1.74	8.58	384	192	0.76	0.60	74.70	
1500	58.41	10.89	1.21	5.83	384	192	0.96	0.75	62.29	
1750	64.78	12.03	1.10	5.16	384	192	1.06	0.83	59.40	
2500	123.73	23.07	1.95	9.21	384	192	2.01	1.58	79.05	
3000	149.88	27.94	2.00	9.26	384	192	2.45	1.92	79.94	●
4400	224.75	41.90	2.10	9.31	384	192	3.68	1.88	81.73	▲
9800	521.67	97.25	2.27	9.01	960	480	3.41	2.67	85.17	▼
30000	1613.49	300.02	2.30	8.14	1024	512	9.88	7.72	85.76	■

Graphite										
Re_b	Re_τ	k^+	$C_f \times 10^2$	$St \times 10^3$	N_x	$N_y = N_z$	Δx^+	$\Delta z^+ = \Delta y^+$	T/τ_t	Symbol
500	33.21	6.61	3.53	17.1	384	192	0.54	0.40	106.28	
1000	47.92	9.53	1.84	8.79	384	192	0.78	0.57	76.68	
1250	56.73	11.29	1.65	7.53	384	192	0.93	0.68	72.66	
1500	73.20	14.55	1.91	8.18	384	192	1.20	0.87	78.08	
2000	104.23	20.72	2.17	10.05	384	192	1.70	1.25	83.38	
2500	133.26	26.49	2.27	10.27	384	192	2.18	1.59	85.29	
3000	162.69	32.34	2.35	10.44	384	192	2.66	1.94	86.77	○
4400	244.54	48.61	2.47	10.60	384	192	3.99	2.92	88.92	△
6000	339.51	67.49	2.56	10.52	512	256	3.70	2.70	90.54	
9800	570.97	113.50	2.72	10.36	960	480	3.73	2.73	93.22	▽
30000	1726.4	343.20	2.65	8.63	1152	576	9.40	6.87	92.07	□

Table 1: Flow parameters for pipes with rough walls.

of smooth channels and pipes[36] , for the sake of achieving convergence of the statistical properties in the cross-stream plane.

3. Results

3.1 Velocity and temperature fields

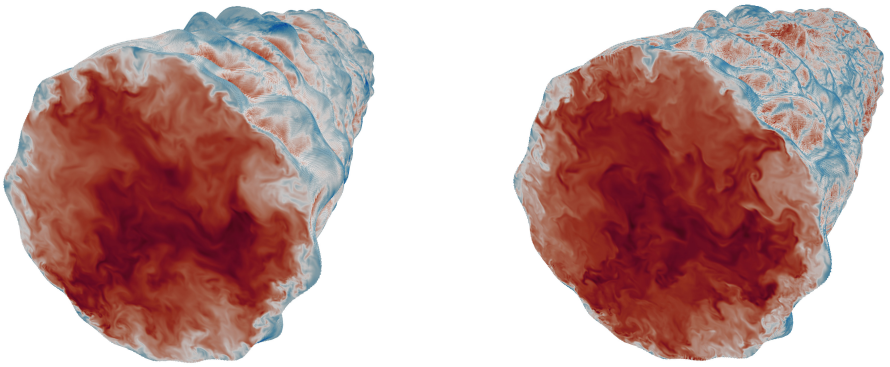

(a) (b)

Figure 2: Instantaneous fields of the streamwise velocity field (a) and of the temperature field (b).

Figure 2 depicts the instantaneous streamwise velocity and temperature fields in the cross-stream section and wall-parallel surface. The instantaneous flow structures are similar for the two fields, the main difference is that the temperature reveals finer and sharper structures owing to absence of the smoothing action of pressure[26] .
Figure 3 shows the mean temperature distribution over the cross section of the pipe, averaged in time and in the streamwise direction, also within the roughness elements. The velocity iso-lines are superimposed on the temperature contours. The contours of the fields do not show any symmetry, thus confirming that for $R/k \lesssim 40$ the effect of the wall is felt throughout the wall layer, as hypotized by Jiménez[18] . Furthermore, the plots show clear sensitivity to

DOI: 10.13009/EUCASS2023-398

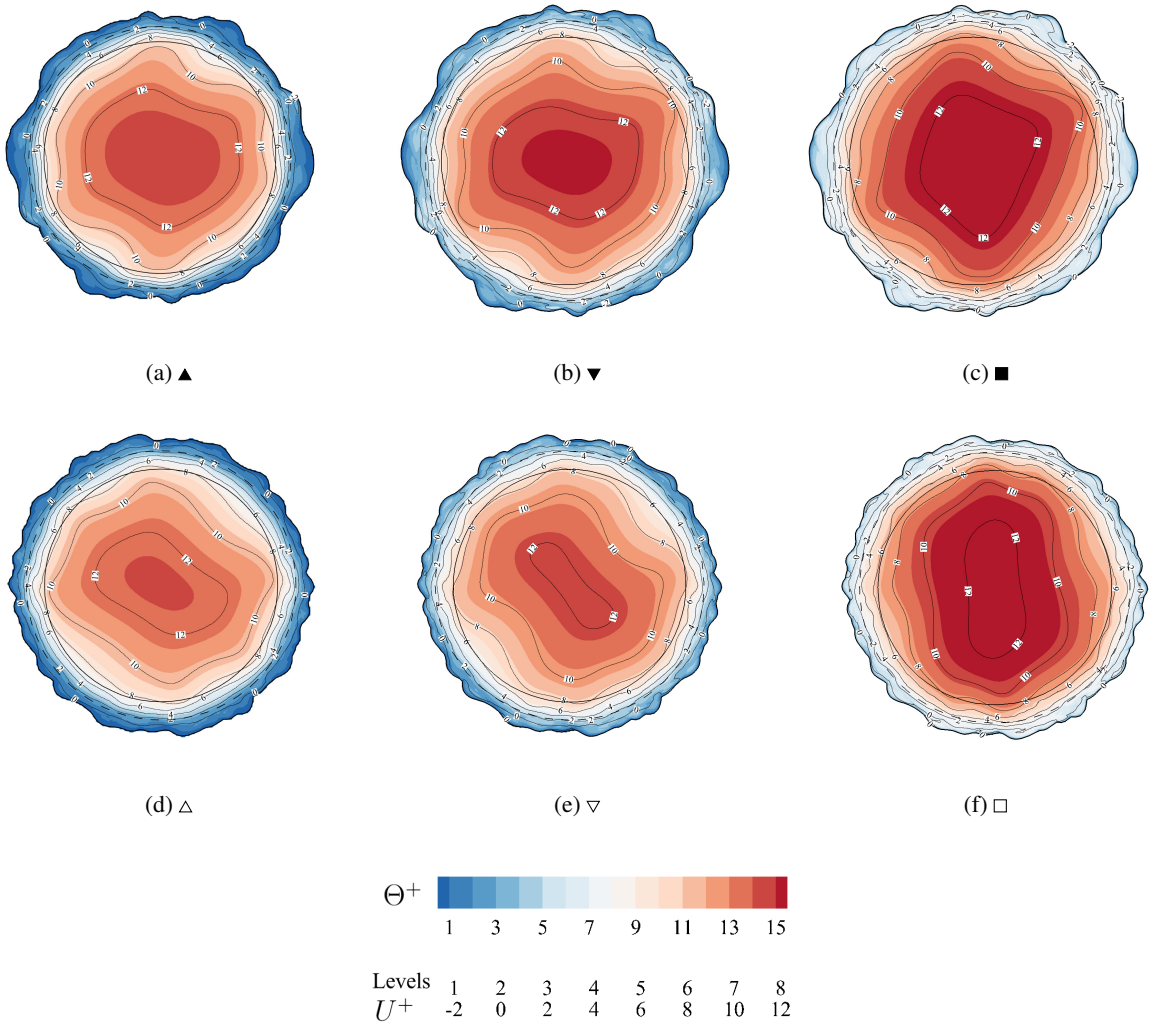

Figure 3: Colored contours of mean temperature, the black lines represent some iso-levels of the mean streamwise velocity. The symbols refer to the flow conditions in table1. The dashed line marks the mean pipe surface and the solid line marks the plane of the crests. The boundary of the maps corresponds to points beyond which no fluid element if found.

Reynolds number variations and to the roughness geometry. As expected, temperature and velocity contours present the same shape far from the wall, however they show some differences in the vicinity of it. These discrepancies are further investigated in figure 4, where we show a scatter plot of mean streamwise velocity and temperature, scaled in inner units. The colors in figure represent the distance from the axis.

The figure shows also the smooth-wall case, in which a near equality of the two distributions occurs. Near the wall a linear relationship between the velocity and temperature fields is expected, i.e. $\Theta^+ = PrU^{+19}$. Also farther from the walls, a linear behaviour is still visible but with a different slope. This can be explained by recalling[35] that in canonical flows the distributions of both velocity and temperature are nearly logarithmic, however with different slopes. In particular, currently accepted values of the Kármán constant are $\kappa = 0.39$ for the mean velocity, and $\kappa = 0.46$ for the mean temperature. As a matter of fact, in the logarithmic region $\Theta^+ = 0.84U^+ - 0.5$ for $Pr = 0.7$.

The rough wall case presents many differences with respect to the smooth pipe. Near the walls (red symbols) a large scatter between Θ^+ and U^+ occurs. This is owed to the presence of the recirculation zones where the velocity reaches negative values, and the temperature remains always positive. The velocity reaches lower negative values for the negative skewed grit-blasted surface, which yields a stronger recirculation zone. The scatter increases with Reynolds bulk for both surfaces. The occurrence of this phenomenon can be attributed to two factors. First, there is an increase of the strength of the recirculation zone which causes a decrease in mean velocity values. Second, there is a significant influx of hotter fluid from the bulk region towards the wall, resulting in elevated mean temperatures within the roughness layer. Far from the wall (blue symbols) the scatter decreases, reflecting also the similarity of the shapes

DOI: 10.13009/EUCASS2023-398

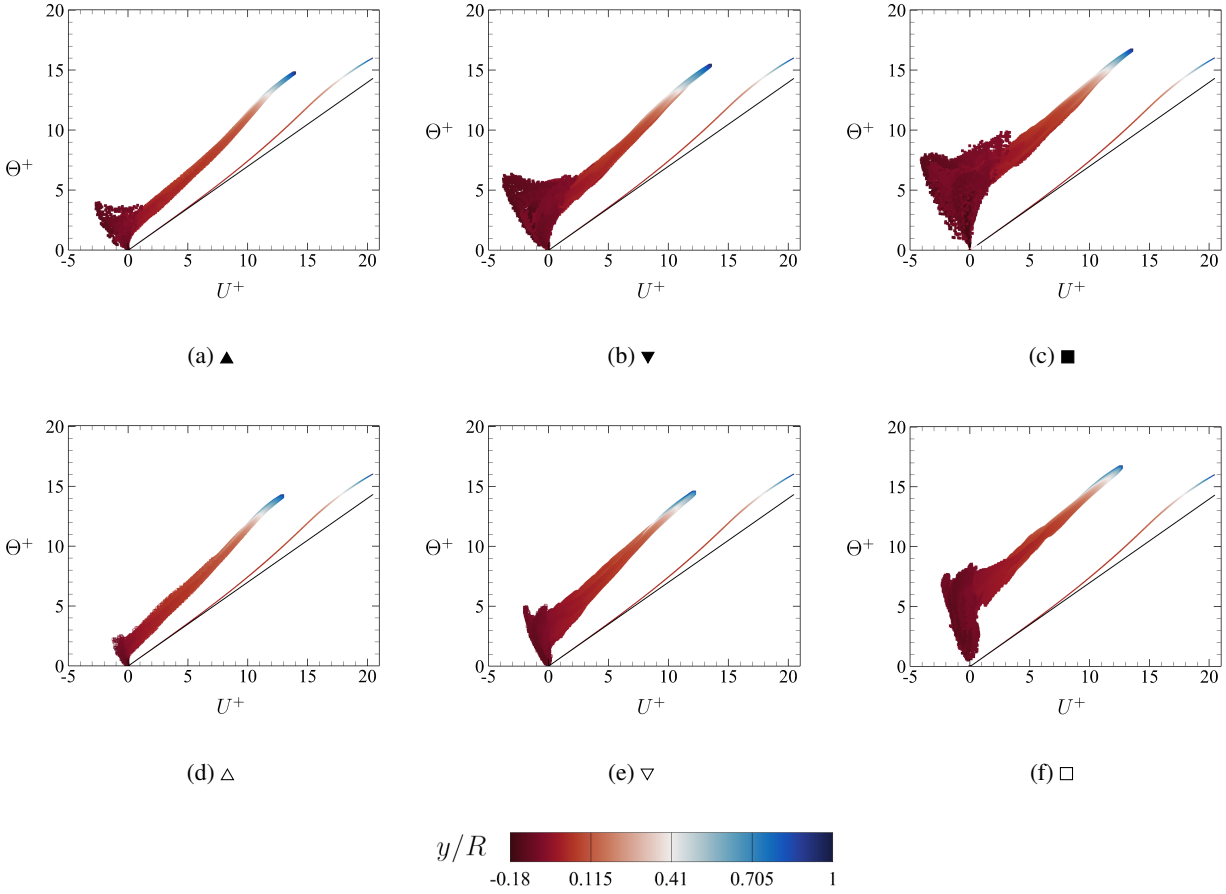

Figure 4: Scatter plot of mean streamwise velocity and temperature. The symbols in the caption refer to the flow conditions in table1. The colors represent the distance from the axis, the black line depicts the relation $\Theta^+ = 0.7U^+$, valid for a smooth pipe near the wall.

of the contours in figure 3. However the intensity of the temperature is much higher than the mean streamwise velocity. Figure 5 depicts the wall-normal profiles of the streamwise velocity and temperature, obtained by further averaging in the azimuthal direction. From now on the solid symbols will be used for the grit-blasted surface and empty symbols for the graphite surface. The figure shows that as k^+ increases, the profiles exhibit a further downward shift within the logarithmic region with respect to the smooth pipe case, resulting in larger velocity and temperature roughness functions. This shift is directly associated with the enhancement of momentum and heat transfer due to roughness. It is evident that the temperature profiles exhibit a slower rate of shift compared to velocity profiles, suggesting that heat transfer is less augmented by roughness compared to momentum transfer. Near the wall, the behaviour is opposite, as DNS at higher k^+ present higher mean velocity and temperature, since the hot flow is capable of penetrating deeper into the roughness canopy[5] . Despite the high relative roughness, a logarithmic layer can still be identified in all cases, with slope similar to the smooth wall case, which allows us to consistently define a roughness function. Given the severe nonuniformities observed in figure 3, the fact that the azimuthally averaged profiles still bear resemblance with those found in the case of smooth walls further points to the importance of the imposed spatially uniform pressure gradient and heat source rather than the local wall conditions. Similar observations were reported by Pirozzoli[37] for flow in smooth square ducts.

3.2 Velocity and temperature roughness functions

In figure 6(a) we show both the velocity and the temperature roughness functions plotted against k^+. The roughness functions of the present DNS have been computed as the log-law shift from the profiles of the smooth case at the same friction Reynolds numbers and the same molecular Prandtl of the rough cases. In figure we also show data from the channel flow DNS of Busse et al.[5] , who used the same two surfaces to investigate two plane rough channels. In this

DOI: 10.13009/EUCASS2023-398

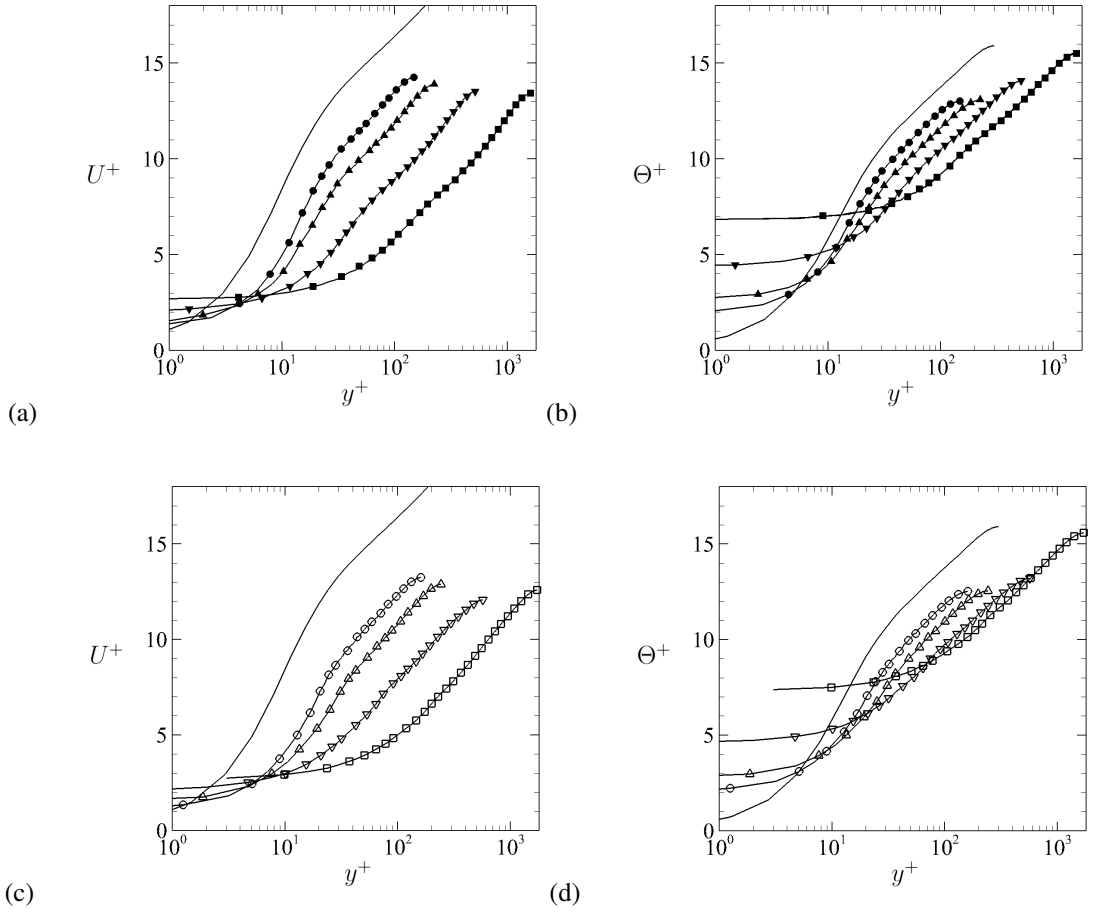

Figure 5: Profiles of streamwise velocity (a,c) and temperature (b,d) for the grit-blasted surface (a,b) and the graphite surface (c,d), symbols as in table 1. The black line without symbols corresponds to the smooth wall case at $Re_b = 9800$ and $Pr = 0.7$.

respect we must specify that we have re-evaluated the data of Busse et al.[5] , since we define the roughness function based on the difference of the velocity profiles within the (narrow) overlap layer, whereas those authors considered the difference of the centreline values. The figure also shows data from Nikuradse's experiment[28] , and Colebrook's relation[8]

$$\Delta U^+ = 1/\kappa \log\left(1 + 0.3k^+\right). \tag{8}$$

First, we notice that the velocity roughness function of the present DNS has a trend quite similar to that observed in Nikuradse's experiments, whereas data depart from Colebrook's relation at $k^+ \lesssim 50$.

For the present simulations, we find that the results at the highest k^+ belong to the fully rough regime, as they appear aligned to the asymptote and exceed $\Delta U^+ = 7$, which is the commonly accepted threshold for achievement of the fully rough regime. Moreover, the trend of the velocity roughness function of the pipes present some differences with respect to the channels of Busse et al.[5] , despite the same rough surface. In particular, in the fully rough regime, this difference is about 5% for given roughness, which points to non-negligible effect of the duct geometry in the presence of large roughness.

The alignment of the the velocity roughness function to the fully-rough asymptote (8) permits to define the sand-grain equivalent roughness height k_s. The latter can be estimated for any kind of rough surface by making the roughness function collapse to Nikuradse's results in this universal regime. For the so called k-type roughness,[18] k_s is proportional to k, and their ratio is referred to as reduction coefficient[38] .

Data fitting of our DNS results yields $k_s^+ \approx 0.76\,k^+$ for the grit-blasted surface, and $k_s^+ \approx 1.0\,k^+$ for the graphite sample. Data fitting of the channel flow DNS results of Busse et al.[5] yields instead $k_s^+ \approx 0.68\,k^+$ for the grit-blasted surface, and $k_s^+ \approx 0.83\,k^+$ for the graphite sample. Once the roughness function is plotted against k_s^+, we note that the trend of

DOI: 10.13009/EUCASS2023-398

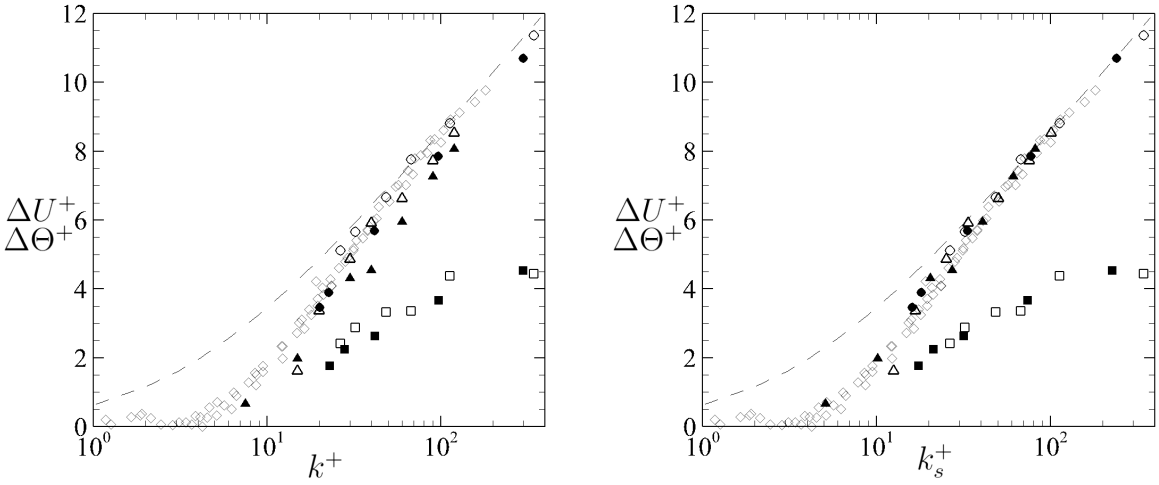

(a) (b)

Figure 6: Variation of velocity and temperature roughness functions with inner-scale roughness height (a) and with equivalent sand-grain roughness height (b). The dashed line denotes Colebrook's relation[8] , $\Delta U^+ = 1/\kappa \log(1 + 0.3k_s^+)$. The diamond-shaped symbols denote data of the velocity roughness function of Nikuradse.[28] The circles denote data of the velocity roughness function of the present pipes: ● grit-blasted surface; ○ graphite surface. The squares denote data of the temperature roughness function of the present pipes: ■ grit-blasted surface; □ graphite surface. The traingles denote data of the velocity roughness function of the channels of Busse et al.:[5] ▲ grit-blasted surface; △ graphite surface.

ΔU^+ collapses to Nikuradse's results throughout, which is a further indication that both surfaces under consideration behave as Nikuradse's roughness.

Last, the figure shows that, as k^+ increases, the velocity roughness function keeps increasing with a steeper slope than the temperature roughness function, which even reaches a plateau at high roughness Reynolds numbers. This hints to the fact that at high Reynolds number the increase in friction with respect to the smooth case is higher than heat transfer augmentation. This topic will be investigated deeply in section 3.3.

3.3 Friction and heat transfer

In figure 7 the friction factors obtained from the present DNS are superposed to Nikuradse's chart. The present friction factors are higher than the ones obtained in the experimental tests because of the larger relative roughness height. In Nikuradse's experiments the friction factor for all surfaces collapsed to the Hagen-Poiseuille prediction $f = 64/Re_b$, in the laminar flow region (the low-Re end of the graph). This suggests that friction is not affected by the change of the wall geometry. In the present DNS we find instead that the computed friction factors are higher than the expected laminar theoretical values by about $5 - 9\%$. This observation suggests that the large relative roughness induces significant changes in the pipe's geometry, consequently leading to modifications within the laminar flow regime as well. Similar findings where reported by Huang et al.[16] , who performed experiments inside pipes with large relative roughness height and found that deviations from the viscous theory appears for $k/R = 0.14$, which is lower than the present values of k/R.

The large relative roughness in the pipe geometries under consideration has the intuitive effect of reducing the available pipe area for fluid flow, thus the effective radius of the pipe is smaller than the geometrical mean radius. To account for this, we define an effective radius to be the hydraulic radius, which is traditionally used for friction prediction in non-circular ducts, and defined as $R_h = 2V/S$, where V is the volume occupied by the fluid, and S is the area of the wetted surface. Figure 7(b) shows the Nikuradse diagram obtained by replacing Re_b with $Re_h = 2R_h u_b/\nu$. In this representation we find that the results collapse to the Hagen-Poiseuille prediction to within less than 1%.

Huang et al.[16] also noticed that the larger the relative roughness, the lower the Reynolds number at which transition from laminar to turbulent regime occurs. This prediction is corroborated by the present data, and in fact transition occurs earlier for the graphite surface than the grit-blasted surface, on account of higher relative roughness. Furthermore, transition is found to occur similarly than in Nikuradse's experiments. Most interestingly, the friction factor past the

DOI: 10.13009/EUCASS2023-398

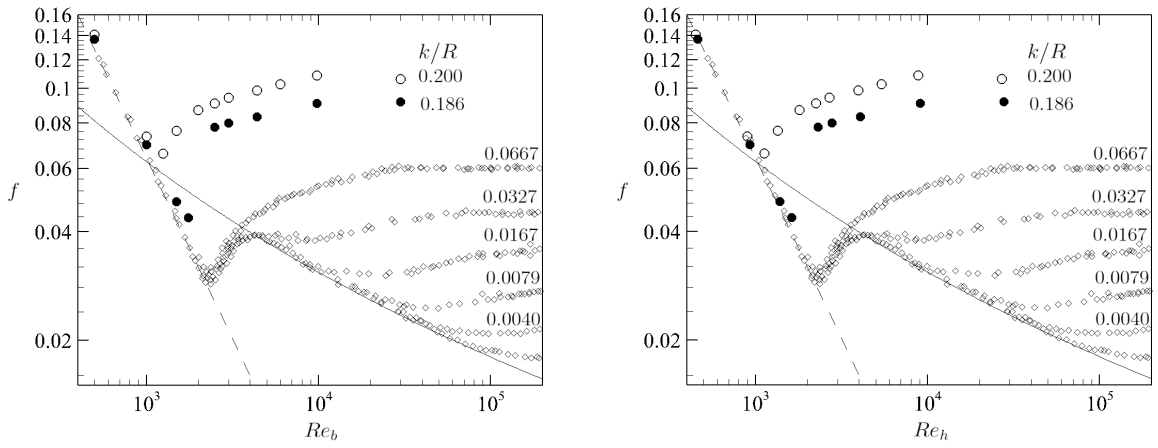

(a) (b)

Figure 7: (a) Variation of friction factor (f) with bulk Reynolds number (Re_b) based on the mean radius (R); (b) Variation of friction factor with the effective bulk Reynolds number (Re_h) based on the effective radius(R_h). Nikuradse's data are shown for pipes with various relative roughness height (k/R). The dashed line denotes the Hagen-Poiseuille $f = 64/Re_b$ friction law, and the solid line Prandtl friction law for turbulent pipe flow. ● depicts the grit-blasted surface; ○ depicts the graphite surface.

transition point is found to increase with the Reynolds number, consistent with numerical simulations in channels with the same roughness geometry[5] . As already mentioned in the previous section, the fully rough regime is established at the highest Reynolds numbers, indeed friction factor shows very small variation with the Reynolds number (also see table 1).

Figure 8 (a) shows the friction coefficient and the Stanton number obtained from the present DNS as functions of the Reynolds numbers. Within the laminar region, it is observed that there exists approximately a 3% disparity in both the friction factor and the Stanton number between the grit-blasted and graphite surfaces, again pointing to the influence of the roughness topography on the cross section of the duct.

As previously mentioned, when the fully rough regime is attained, the friction coefficient C_f reaches a constant value. Since the Stanton number is the thermal counterpart of the friction coefficient, one would also expect a constant value of the Stanton number in the fully rough regime. However the plot shows that St decreases at the highest Reynolds numbers. Furthermore, the Stanton number is almost constant in the transitional rough regime, as if the fully rough regime is reached at lower Reynolds number for the temperature field. Similar results have been found by Forooghi et al.[13] , who addressed this behaviour to the thinner boundary layer of the temperature with respect to the velocity at Prandtl 0.7.

Figure 8 (b) shows the trend of the Reynolds Analogy Factor ($RAF = 2St/Cf$) of the rough pipes over the one of the smooth-wall pipe (RAF_S) as a function of Reynolds bulk in the turbulent regime. The Stanton number for the smooth case is computed based on the correlation of Dittus and Boelter[10] and the friction coefficient is evaluated by an interpolation of the data of Pirozzoli et al.[36] . RAF_S is computed at the same Reynolds bulk of the rough case. In accordance with previous studies[2,13] , the RAF decreases with respect to the smooth pipe, this is due to the fact that roughness augments momentum transfer more than heat transfer. As the Reynolds number increases, the efficiency in heat transfer decreases and so does RAF. Indeed, at low Re_b the viscous transport is still important, hence the value of RAF is closer to that of a smooth wall. Whereas, in the fully rough regime the viscous sub-layer is disrupted, and the flow resistance mainly arises from pressure or form drag rather than viscous drag. However, there is no enhancement mechanism for heat transfer comparable to the pressure, this explains why heat transfer is not increased by roughness as much as skin friction, especially for high Reynolds numbers and large roughness[13,23,24,34] .

DOI: 10.13009/EUCASS2023-398

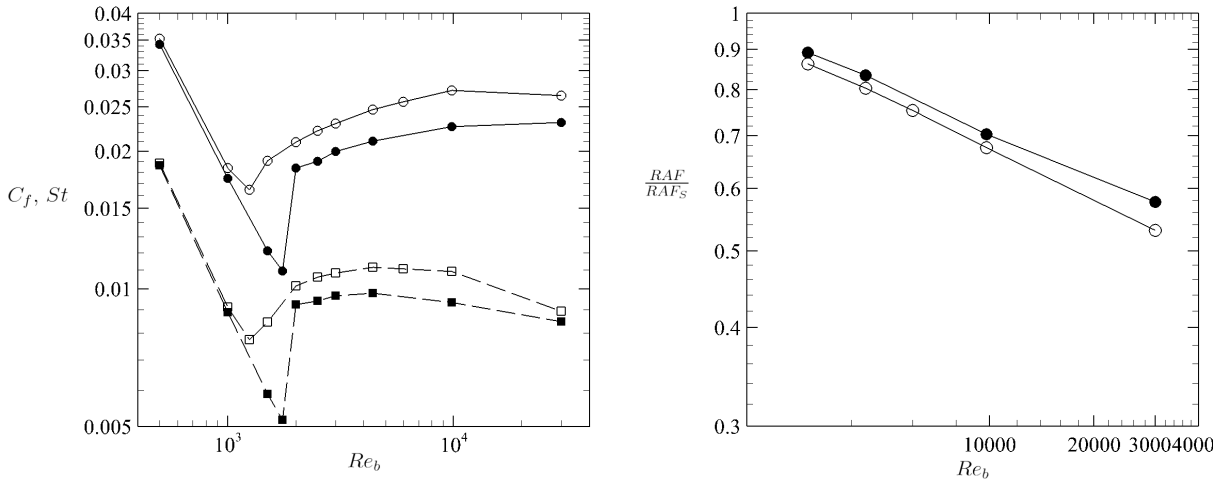

Figure 8: (a) The circles depict the friction coefficient (C_f) and the squares show the Stanton number (St) as functions of bulk Reynolds number (Re_b); (b) Ratio of the Reynolds Analogy factor for the rough case (RAF) and for the smooth wall case (RAF_S), plotted against the bulk Reynolds number (Re_b). The solid symbols depicts the results for the grit-blasted surface, whereas the empty ones denote the graphite surface.

4. Conclusions

We have carried out DNS of flow through rough pipes for two types of rough surfaces, focusing on the influence of large relative roughness on both momentum and heat transfer.

First, it is evident that the presence of rough surfaces influences both the velocity and the temperature fields also far from the wall. Nonetheless, it is still possible to define a logarithmic region for the streamwise velocity and temperature profiles of the rough pipes, which runs parallel to the profiles of the smooth pipes. This enables the computation of roughness functions and the determination of the sand-grain equivalent roughness height by enforcing universality within the fully rough regime.

Moreover, the data indicates that both surfaces exhibit behavior similar to Nikuradse's roughness, despite the significant alteration of the pipe's cross-sectional shape caused by the large roughness height. Indeed, the latter results in higher friction coefficient values in the laminar region compared to the theoretical values. In addition,we found smaller critical Reynolds numbers at which the transition from laminar to turbulent flow occurs. Moreover, from the inspection of the velocity roughness function, we can notice that the present results differ from the ones of Busse et al.[5] of about 5%, confirming that the large roughness modifies the cross-sectional shape of the pipe.

The large roughness height generates dissimilarities between the velocity and temperature fields, especially near the wall. The presence of recirculation zones in fact makes the hot flow penetrate deeper in the roughness canopy and this determines higher values of temperature near the wall with respect to velocity, which can also reach negative values. Moreover, it was noted that the temperature roughness function presents lower values than the velocity, meaning that some differences occur also in the logarithmic region, where these quantities have been computed. Specifically, the temperature roughness function deviates from the velocity when plotted against k^+, reaching a plateau. This result is associated with the breakdown of the Reynolds analogy at higher Reynolds numbers. Indeed, heat and momentum transfer exhibit significant disparities, leading to a reduction in heat transfer efficiency. This phenomenon arises from the fact that, at high Reynolds numbers, the resistance of the flow is mainly owed to the pressure and not to the viscous drag. However, there is no enhancement mechanism for heat transfer such as pressure. This yields a higher increase of the C_f than the St number.

Follow-up studies should include more DNS of realistic rough surfaces, to understand how the type of roughness influences heat transfer.

DOI: 10.13009/EUCASS2023-398

5. Acknowledgments

We acknowledge that the results reported in this paper have been achieved using the PRACE Research Infrastructure resource GALILEO100 based at CINECA, Casalecchio di Reno, Italy. The authors would like to thank Neil Sandham and co-workers for making available the roughness geometries. This work received funding from AVIO SpA and from Regione Lazio in the form of the PhD scholarship of the leading author.

References

[1] M. Bernardini, D. Modesti, and S. Pirozzoli. On the suitability of the immersed boundary method for the simulation of high-Reynolds-number separated turbulent flows. *Comp. Fluids*, 130:84–93, 2016.

[2] J. Bons. A critical assessment of reynolds analogy for turbine flows. *J. Heat Transfer*, 127(5):472–485, 2005.

[3] P. Burattini, S. Leonardi, P. Orlandi, and R.A. Antonia. Comparison between experiments and direct numerical simulations in a channel flow with roughness on one wall. *J. Fluid Mech.*, 600:403–426, 2008.

[4] A. Busse, M. Lützner, and N.D. Sandham. Direct numerical simulation of turbulent flow over a rough surface based on a surface scan. *Comput. Fluids*, 116:129–147, 2015.

[5] A. Busse, M. Thakkar, and N.D. Sandham. Reynolds-number dependence of the near-wall flow over irregular rough surfaces. *J. Fluid Mech.*, 810:196–224, 2017.

[6] F. Calignano, D. Manfredi, E.P. Ambrosio, L. Iuliano, and P. Fino. Influence of process parameters on surface roughness of aluminum parts produced by dmls. *J. Adv. Manuf. Technol.*, 67(9):2743–2751, 2013.

[7] L. Chan, M. MacDonald, D. Chung, A. N. Hutchins, and Ooi. A systematic investigation of roughness height and wavelength in turbulent pipe flow in the transitionally rough regime. *J. Fluid Mech.*, 771:743–777, 2015.

[8] C.F. Colebrook, T. Blench, H. Chatley, E.H. Essex, J.R. Finniecome, G. Lacey, J. Williamson, and G.G. Macdonald. Correspondence. turbulent flow in pipes, with particular reference to the transition region between the smooth and rough pipe laws.(includes plates). *J. Inst. Civ. Eng.*, 12(8):393–422, 1939.

[9] D.F. Dipprey and R.H. Sabersky. Heat and momentum transfer in smooth and rough tubes at various prandtl numbers. *Int. J. Heat Mass Transf.*, 6(5):329–353, 1963.

[10] F.W. Dittus and L.M.K. Boelter. Heat transfer in automobile radiators of the tubular type. *Int. Commun. Heat Mass Transf.*, 12(1):3–22, 1985.

[11] P. Forooghi, M. Stripf, and B. Frohnapfel. A systematic study of turbulent heat transfer over rough walls. *Int. J. Heat Mass Transf.*, 127:1157–1168, 2018.

[12] P. Forooghi, A. Stroh, F. Magagnato, S. Jakirlić, and B. Frohnapfel. Toward a universal roughness correlation. *J. Fluids Eng.*, 139(12), 2017.

[13] P. Forooghi, A. Weidenlener, F. Magagnato, B. Böhm, H. Kubach, T. Koch, and B. Frohnapfel. Dns of momentum and heat transfer over rough surfaces based on realistic combustion chamber deposit geometries. *Int. J. Heat Fluid Flow*, 69:83–94, 2018.

[14] F.R. Hama. Boundary layer characteristics for smooth and rough surfaces. *Trans. Soc. Nav. Arch. Marine Engrs.*, 62:333–358, 1954.

[15] F. Harlow and J. Welch. Numerical calculation of time-dependent viscous incompressible flow of fluid with free surface. *Phys. Fluids*, 8(12):2182, 1965.

[16] K. Huang, J.W. Wan, C.X. Chen, Y.Q. Li, D.F. Mao, and M.Y. Zhan. Experimental investigation on friction factor in pipes with large roughness. *Exp. Therm. Fluid Sci.*, 50:147–153, 2013.

[17] G. Iaccarino and R. Verzicco. Immersed boundary technique for turbulent flow simulations. *Appl. Mech. Rev.*, 56(3):331–347, 2003.

[18] J. Jiménez. Turbulent flows over rough walls. *Annu. Rev. Fluid Mech.*, 36:173–196, 2004.

DOI: 10.13009/EUCASS2023-398

[19] B.A. Kader. Temperature and concentration profiles in fully turbulent boundary layers. *Int. J. Heat Mass Transf.*, 24(9):1541–1544, 1981.

[20] B.A. Kader and A.M. Yaglom. Heat and mass transfer laws for fully turbulent wall flows. *Int. J. Heat Mass Trans.*, 15(12):2329–2351, 1972.

[21] W.M. Kays and E.Y. Leung. Heat transfer in annular passages-hydrodynamically developed turbulent flow with arbitrarily prescribed heat flux. *Int. J. Heat Mass Transf.*, 6(7):537–557, 1963.

[22] J. Kim and P. Moin. Application of a fractional-step method to incompressible Navier-Stokes equations. *J. Comput. Phys.*, 59:308–323, 1985.

[23] Y. Kuwata. Direct numerical simulation of turbulent heat transfer on the reynolds analogy over irregular rough surfaces. *Int. J. Heat Fluid Flow*, 92:108859, 2021.

[24] S. Leonardi, P. Orlandi, L. Djenidi, and R.A. Antonia. Heat transfer in a turbulent channel flow with square bars or circular rods on one wall. *J. Fluid Mech.*, 776:512–530, 2015.

[25] R.C. Martinelli. Heat transfer to molten metals. *Trans. Am. Soc. Mech. Eng.*, 69(8):947–956, 1947.

[26] Davide Modesti and Sergio Pirozzoli. Direct numerical simulation of forced thermal convection in square ducts up to. *Journal of Fluid Mechanics*, 941:A16, 2022.

[27] F. Nasuti, A. Torricelli, and S.Pirozzoli. Conjugate heat transfer analysis of rectangular cooling channels using modeled and direct numerical simulation of turbulence. *Int. J. Heat Mass Transf.*, 181:121849, 2021.

[28] J. Nikuradse. *Untersuchung über die Geschwindigkeitsverteilung in turbulenten Strömungen*. Vdi-verlag, 1926.

[29] J. Nikuradse. Strömungsgesetze in rauhen rohren. vdi-forsch, 1933.

[30] W. Nunner. *Heat transfer and pressure drop in rough tubes*. Atomic Energy Research Establishment, 1958.

[31] P. Orlandi. *Fluid flow phenomena: a numerical toolkit*, volume 55. Springer Science & Business Media, 2000.

[32] P. Orlandi and S. Leonardi. Dns of turbulent channel flows with two-and three-dimensional roughness. *J. Turbul.*, 7:N73, 2006.

[33] Joseph o'Rourke et al. *Computational geometry in C*. Cambridge University press, 1998.

[34] J.W.R. Peeters and N.D. Sandham. Turbulent heat transfer in channels with irregular roughness. *Int. J. Heat Mass Transf.*, 138:454–467, 2019.

[35] S. Pirozzoli, M. Bernardini, and P. Orlandi. Passive scalars in turbulent channel flow at high Reynolds number. *J. Fluid Mech.*, 788:614–639, 2016.

[36] S. Pirozzoli, J. Romero, M. Fatica, R. Verzicco, and P. Orlandi. Dns of passive scalars in turbulent pipe flow. *J. Fluid Mech.*, 940:A45, 2022.

[37] Sergio Pirozzoli. On turbulent friction in straight ducts with complex cross-section: the wall law and the hydraulic diameter. *Journal of Fluid Mechanics*, 846:R1, 2018.

[38] H. Schlichting. Experimentelle untersuchungen zum rauhigkeitsproblem. *Ing. Arch.*, 7(1):1–34, 1936.

[39] H. Schlichting. Boundary layer theory. *McGraw-Hill, New York*, 1979.

[40] J.C. Snyder, C.K. Stimpson, K.A. Thole, and D. Mongillo. Build direction effects on additively manufactured channels. *J. Turbomach.*, 138(5):051006, 2016.

[41] C.K. Stimpson, J.C. Snyder, K.A. Thole, and D. Mongillo. Roughness effects on flow and heat transfer for additively manufactured channels. *J. Turbomach.*, 138(5):051008, 2016.

[42] M. Thakkar, A. Busse, and N. Sandham. Dataset for surface correlations of hydrodynamic drag for transitionally rough engineering surfaces. `https://eprints.soton.ac.uk/392562/`, 2016.

[43] M. Thakkar, A. Busse, and N. Sandham. Surface correlations of hydrodynamic drag for transitionally rough engineering surfaces. *J. Turbul.*, 18(2):138–169, 2017.